Air cooled bainitic steels for strong, seamless pipes
Part 1 – alloy design, kinetics and microstructure

G. Gomez[1], T. Pérez[1] and H. K. D. H. Bhadeshia*[2]

Seamless pipes are usually quenched and tempered after manufacture in order to obtain the desired properties. The possibility of avoiding this heat treatment is explored here, by designing steels which transform into an carbide free bainitic microstructure during cooling from the hot processing phase of the pipe. The cooling conditions studied are appropriate for the manufacturing process and care has been taken to ensure that the correct microstructure is generated for the range of cooling rates experienced in industrial practice. The alloy design has been validated by kinetic and microstructural studies.

Keywords: Seamless pipe, Bainite, Retained austenite, Incomplete reaction

Introduction

Seamless pipes for applications in the oil and gas industries are made from steel in the quenched and tempered martensitic condition. This heat treatment adds to cost and it is difficult to ensure a uniform microstructure when making pipes with thick walls.[1] An alternative scenario which avoids both of these difficulties would be to allow a carbide free bainitic microstructure to evolve directly after the production of the seamless pipe as it cools to ambient temperature. With careful design, such microstructures have previously been shown to result in a good combination of strength and toughness in both steels[2–12] and cast irons.[13–15]

The purpose of the present work was to see whether this microstructure could be made by continuous cooling transformation under conditions appropriate for the manufacture of seamless pipes. The property requirements are a proof strength in excess of 1000 MPa with a ductile brittle transition temperature below -20°C (with a minimum Charpy value of 21 J and a minimum average of 24 J). After hot rolling, the pipes are currently heat treated by quenching to martensite and tempering. It would clearly be an advantage to eliminate the need for this heat treatment. As will be seen later, the properties required are demanding. Promising alloys have been developed in previous work and in another application concept, in which the mixture of bainitic ferrite and carbon enriched retained austenite was generated during cooling to give yield strength >1100 MPa and a fracture toughness in excess of 160 MPa m$^{1/2}$.[16,17] The cooling conditions, sample dimensions and fabrication procedures for those alloys differ from that during pipe manufacture but the previous work provides a foundation from which to proceed.

Part 1 of the study deals with alloy design, transformation kinetics and microstructure, Part 2 with the mechanical properties achieved.

Alloy design

The alloy design was aimed at producing a microstructure composed of bainitic ferrite and films of retained austenite during air cooling from the austenite phase field. Finite element thermal calculations indicated that for tube thicknesses between 8 and 24 mm, the average cooling rate in air on exiting the hot rolling mill (finish rolling temperature: 950–1000°C) is 0·1–0·5 K s^{-1}. It was judged that to achieve a fine microstructure requires a bainite start temperature $B_S<500^{\circ}$C, which should also help avoid products such as allotriomorphic ferrite, pearlite and Widmanstätten ferrite at the expected cooling rates.

The design criteria for the steels include the following:

(i) sufficient silicon or aluminium addition to avoid the precipitation of cementite during the bainite reaction, thus allowing the carbon to be retained within the residual austenite[18–21]

(ii) the extent of transformation should be such that blocky regions of austenite are avoided in the final microstructure;[3,4] this can be achieved by ensuring that the carbon concentration that the austenite can tolerate, x_{T_0}, before diffusionless transformation becomes impossible is at a maximum. Substitutional solute concentrations

[1]Department of Metallurgy, Tenaris Argentina R&D Simini 250, 2804 Campana, Pcia, Buenos Aires, Argentina
[2]Materials Science and Metallurgy, University of Cambridge Cambridge CB2 3QZ, UK

*Corresponding author, email hkdb@cam.ac.uk

Published by Maney on behalf of the Institute
Received 16 August 2008; accepted 6 October 2008
DOI 10.1179/174328408X388130

can be adjusted to maximise x_{T_0} as described elsewhere[3,4,16,17]

(iii) the microstructure should be as fine as possible in order to achieve the required strength. This is usually achieved by suppressing the transformation temperature, increasing the strength of the austenite and enhancing the driving force for transformation.[22–24] Toughness is also enhanced by refining the microstructure because the transformation of carbon enriched austenite into coarse, untempered martensite can otherwise lead to spontaneous cracking.[25] Notice that although large quantities of carbon can be added to suppress the transformation temperature and obtain nanocrystalline bainite, the strength would then become excessive for the seamless pipe application; furthermore, the transformation times required would make this particular application impractical.[26]

The goal of the present work was to obtain a proof strength in excess of 1000 MPa whilst meeting the pipe Charpy toughness requirements, and for the processing conditions outlined above. Thus, the nickel containing steels in[16] formed the starting point of the design process (Table 1). Time temperature transformation diagrams were calculated as in Refs. 27–29 and these were converted into continuous cooling transformation (CCT) diagrams assuming the Schiel additivity principle.[30] Two compositions were selected for manufacture (Table 1); the significant difference between these is the carbon concentration. The concentration of manganese was kept to a practical low limit (0·1 wt-%) in order to avoid banding due to solidification induced chemical segregation; such banding can have a detrimental effect on the mechanical properties since the Mn enriched regions remain martensitic on cooling.[31] Figure 1 shows the such banding has successfully been avoided. Nickel, on the other hand, helps improve the toughness of ferrite.[32,33] The chromium concentration was reduced in order to maximise the amount of bainitic transformation and aluminium was permitted in small concentrations for the purposes of steel deoxidation. The molybdenum addition is there to combat austenite grain boundary embrittlement due to impurities such as phosphorus.[34,35]

Figure 2 shows the calculated transformation start temperatures as a function of the cooling rate. It is therefore expected that both steels would present predominantly bainitic microstructures during cooling at 0·1–0·5 K s^{-1}. Some allotriomorphic ferrite is possible at the lower end of this cooling range (0·1–0·2 K s^{-1}) but this is expected to be minimal given the high hardenability of the steel. The calculated B_S temperatures were $<500^\circ$C in both cases: 471 and 446°C for alloys 1 and 2 respectively. The effect of carbon is to suppress transformation temperatures at all cooling rates, so a finer microstructure is expected in alloy 2.

Experimental

The alloys were prepared as 20 kg melts (Table 1) in a vacuum induction furnace. The materials were electroslag remelted in order to reduce the sulphur content. Slabs of 140 mm thickness were cropped to 123 mm thickness due to limitations in the pilot mill and then hot rolled into plates of 16 mm thickness. During rolling the reheating and finish rolling temperatures were chosen to be 1250 and 1000°C to approximately match those used during the industrial processing of pipes. After hot rolling the plates with dimensions $800 \times 170 \times 16$ mm were air cooled to room temperature.

Hardness, tensile and impact tests were conducted on the as rolled samples. Cylindrical samples of 8·9 mm diameter and 35 mm of guage length were used for tensile testing, with the results in each case averaged over two samples. Charpy V notch tests were conducted on full size samples ($10 \times 10 \times 55$ mm) machined in the transverse direction ('T–L' according to ASTM E23). The reported impact results correspond to average values over three measurements for each temperature, which ranged from room temperature to −40°C. The

Table 1 Alloy compositions (in wt-%) austenite grain size measured as mean lineal intercept $\bar{L}_\gamma$ (in μm) and volume fraction V_γ of retained austenite: in case of Gleeble samples, cooling rates associated with each V_γ value are also stated; data for as rolled samples will be discussed in Part 2 (Ref. 36)

		Alloy 1		Alloy 2	
	Previous[16]	Specified	Actual	Specified	Actual
C	0·30	0·25	0·24	0·30	0·30
Mn	–	0·1	0·09	0·1	0·10
Si	1·5	1·40	1·27	1·40	1·42
Cr	1·44	1·00	1·00	1·00	1·03
Mo	0·25	0·25	0·23	0·25	0·22
Ni	3·5	3·60	3·64	3·60	3·48
Al		0·03	0·014	0·03	0·040
S		<0·002	0·001	<0·002	0·002
P		<0·01	0·005	<0·01	0·01
N		<0·006	0·0063	<0·006	0·0023
O		<0·003	0·0014	<0·003	0·0011
$\bar{L}_\gamma$ (as rolled)		52±10		39±11	
$\bar{L}_\gamma$ (normalised)		22±3		16±4	
$\bar{L}_\gamma$ (Gleeble)		47±12		36±10	
V_γ (as rolled)		0·18±0·01		0·13±0·01	
V_γ (Gleeble, 0·1 K s^{-1})		0·28±0·03		0·27±0·03	
V_γ (Gleeble, 0·2 K s^{-1})		0·18±0·03		0·15±0·03	
V_γ (Gleeble, 0·5 K s^{-1})		0·10±0·02		0·05±0·02	
V_γ (Gleeble, 2·0 K s^{-1})		–		–	

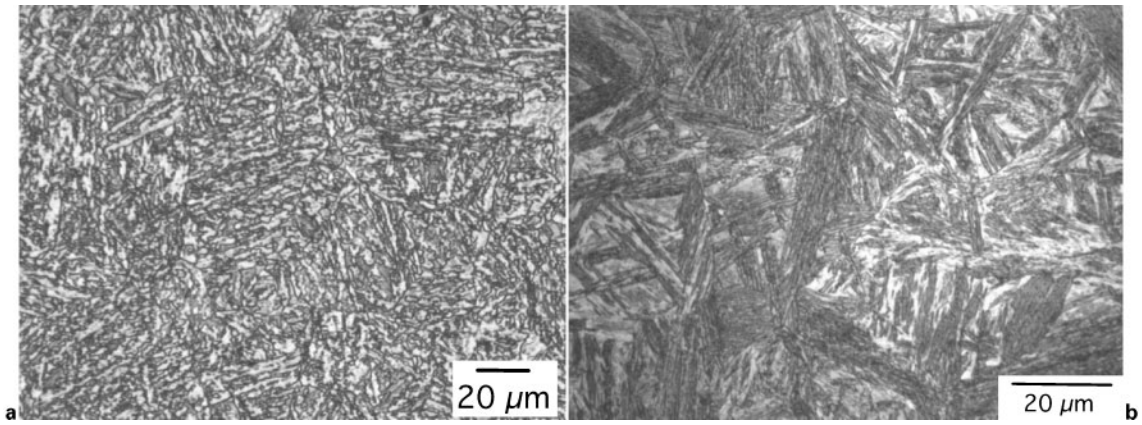

1 Optical micrographs from hot rolled states of *a* alloy 1 and *b* alloy 2, showing absence of microstructural banding

percentage of ductile fracture on the broken Charpy specimens was measured according to standard practice[37] following industrial specifications. Vickers hardness was measured using a 20 kg load, and averaged over five measurements at random positions.

Optical and scanning electron microscopy studies were on cold mounted, ground and polished samples and etched in 2% nital. The amount of retained austenite in the hot rolled samples[36] was determined using quantitative X-ray analysis on a Phillips X'Pert diffractometer and unfiltered Cu K_α radiation. The scanning speed was 0·1 K min^{-1} over the range $2\theta = 30$–110°. The machine was operated at 40 kV and 40 mA. The retained austenite content was calculated from the integrated intensities of (111), (002), (022), (113) and (222) austenite peaks, and those of (011), (002), (112) and (022) planes of ferrite, using Rietveld analysis. The reheated Gleeble samples were, because of their small size, analysed using just two peaks $(111)_\gamma$ and $(011)_\alpha$ by scanning over $2\theta = 40$–55° at the same speed, so in this case the results are less accurate but should indicate any trends correctly.

Continuous cooling transformation diagrams were determined from dilatometric tests performed in a Gleeble 3500 thermomechanical simulator, using 6 mm diameter cylindrical samples heated at 5 K s^{-1} up to 1000°C (chosen to match the austenite grain size to the rolled plates), followed immediately by cooling at a fixed rate down to room temperature. The tests were conducted in a vacuum purged chamber under flowing high purity argon containing 5% hydrogen to prevent decarburisation and oxidation. The temperature evolution was followed with a type *K* type thermocouple spot welded on the surface of the specimen, in its middle section. The changes in sample diameter were acquired as a function of time with a high resolution dilatometer at the location of the thermocouple (the accuracy of the measurement was $\pm 0{\cdot}1$ μm). Cooling rates in the range 0·1–5°C were used to construct CCT diagrams and the fraction of transformation was determined by applying the lever rule to the dilatometer reading relative to the austenite and ferrite lines from regions where transformation was absent. The Vickers hardness was measured using a 10 kg load, and averaged over at least three measurements at random positions in each case.

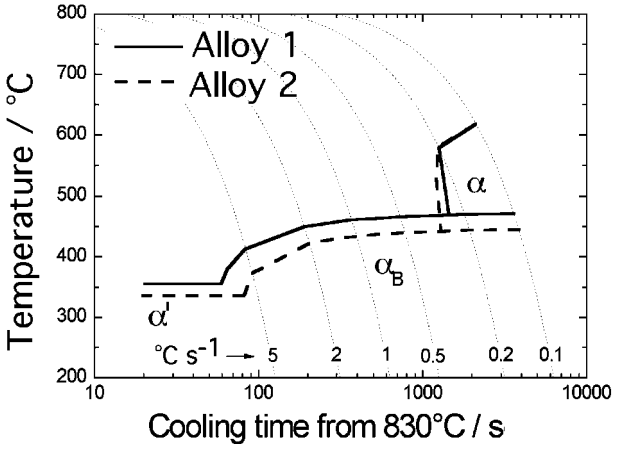

2 Calculated transformation start temperatures for alloys 1 and 2: α, α_B and α' stand for allotriomorphic ferrite, bainite and martensite respectively

The tempering behaviour was studied on samples $20 \times 20 \times 8$ mm, sealed in quartz tubes containing a partial pressure of argon, at temperatures between 250 and 500°C for 1 h. Further heat treatments were carried out on $200 \times 170 \times 16$ mm plates which were then machined into tensile and impact test samples:

(i) alloy 1, 880°C for 15 min followed by air cooling (normalising)
(ii) alloy 2, 840°C for 15 min followed by air cooling (normalising)
(iii) alloy 2, tempering at 300°C for 1 h, followed by air cooling
(iv) alloy 2, tempering at 500°C for 30 min followed by air cooling.

Transmission electron microscopy was conducted on a JEOL 2000FX transmission electron microscope operating at 200 kV. Thin foil preparation methods have been described elsewhere.[38]

Continuous cooling transformation diagrams

Examples of the raw data obtained from Gleeble tests are presented in Fig. 3 for two cooling rates. Austenite formation began on heating at $A_{c1} = 725$ and 735°C for alloys 1 and 2 respectively, and finished at $A_{c3} = 835$–845°C for alloy 1 and or 820–830°C for alloy 2. The maximum reheating temperature of 1000°C is far above A_{c3} leading to relatively coarse austenite grains. The measured austenite grain sizes are given in Table 1; it is important to note that the Gleeble samples have

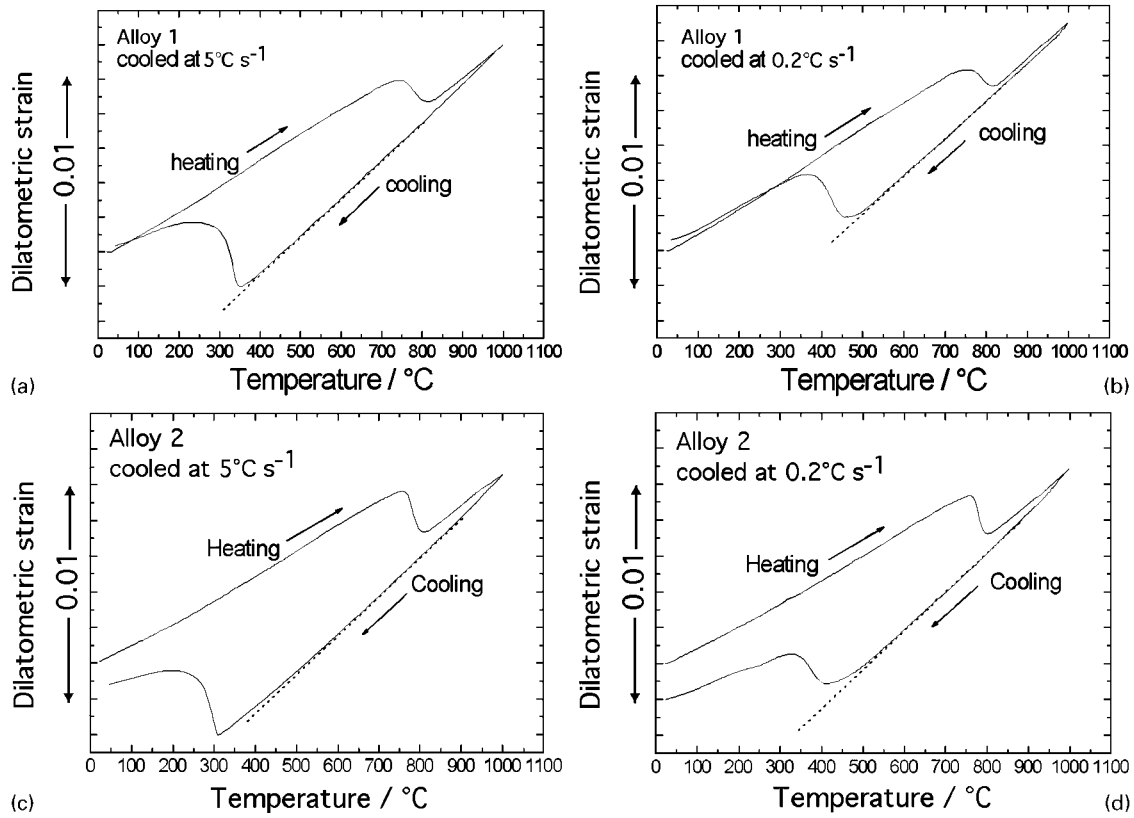

a,b alloy 1; *c,d* alloy 2

3 Typical dilatometric data

essentially the same $\overline{L}_\gamma$ as the as rolled specimens so that the CCT diagrams are representative of the rolled condition. The reason why $\overline{L}_\gamma$ for alloy 2 is consistently smaller than that for alloy 1 is not clear, but it is speculated that the reduction is associated with its higher aluminium concentration which via the formation of aluminium nitride, acts to refine the grain size.[39–42]

The dilatometric measurements following austenitisation at 1000°C in combination with microscopy were used to measure the CCT diagrams illustrated in Fig. 4. The temperatures corresponding to 5, 10, 50 and 90% of transformation are plotted as a function of the cooling time from 830°C (the approximate temperature at which phase transformation can begin). In some cases a surface decarburised layer some 70 μm thickness occurred, which represented about 0·03 volume fraction of the sample; this is why at 1% transformation temperature is not represented in Fig. 4.

The M_S temperatures were determined from the change in the slope of the transformation strain versus temperature curve during continuous cooling. M_S is not plotted for alloy 1 because fully martensitic transformation was not obtained for the cooling rates studied; transformation during cooling at 5 K s^{-1} began at ~500°C although in excess of 95% of the reaction occurred <350°C when an abrupt rise in decomposition rate of austenite was noted in the dilatometric curve. This is consistent with the M_S temperature in the range 350–355°C calculated as in Refs. 28 and 29 and using the Andrews equation.[43] The extent of transformation above the calculated M_S increased as the cooling rate decreased and typical microstructures for the slow cooling rates of relevance are illustrated in Fig. 5. At

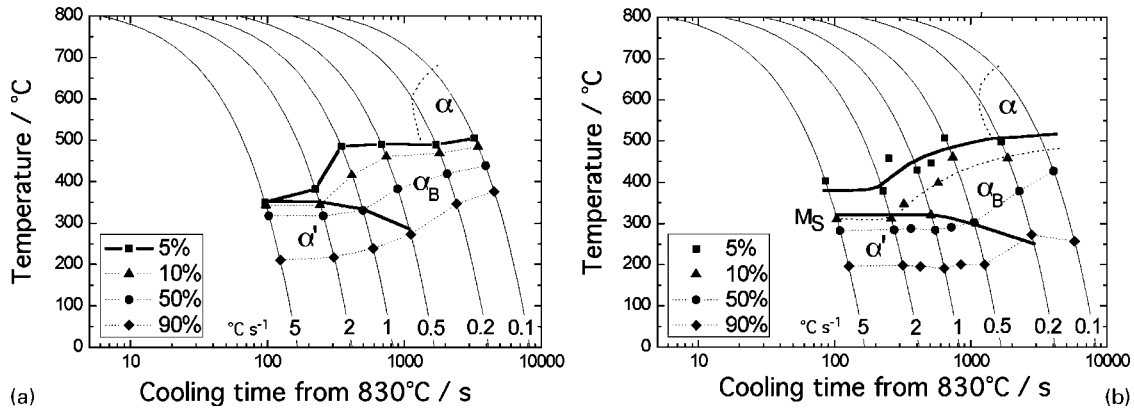

a alloy 1, austenitised at 1000°C; *b* alloy 2, austenitised at 1000°C

4 Measured CCT diagrams

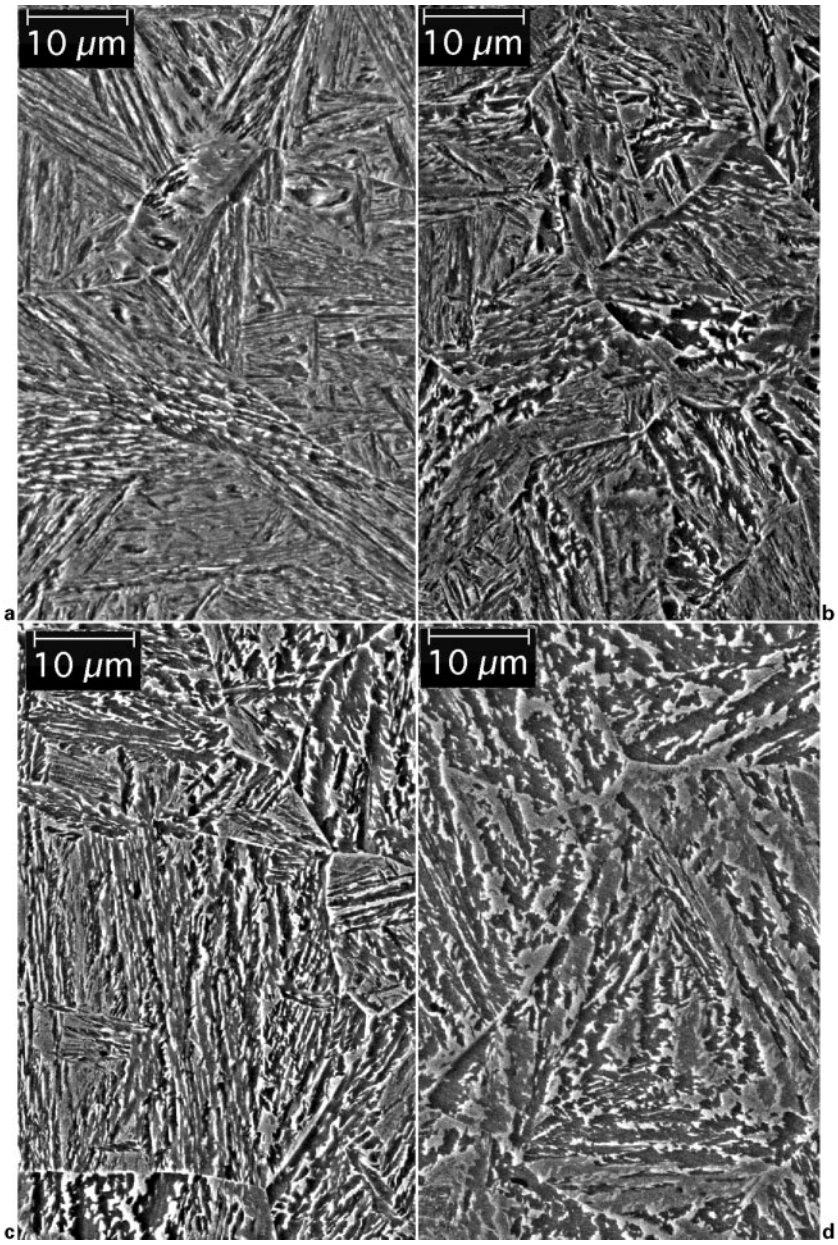

a 1 K s^{-1}; *b* 0·5 K s^{-1}; *c* 0·2 K s^{-1}; *d* 0·1 K s^{-1}

5 Alloy 1

0·5 K s^{-1} most of the transformation took place above the M_S and below the calculated B_S (471°C). The same occurred when cooling at 0·2 K s^{-1}, as is clear from the dilatometric curve in Fig. 3. The appearance of bainite was confirmed metallographically, as shown in Fig. 5. Allotriomorphic ferrite observed at 0·2 and 0·1 K s^{-1} but the fraction was <0·05 as estimated using point counting.[44]

The retained austenite contents reported in Table 1 are generally consistent with the dilatometric analysis; V_γ decreases as the cooling rate is increased because bainite then has less time to form, thus resulting in a greater tendency to form martensite. Alloy 2 in general has a smaller fraction of austenite, consistent with its greater hardenability (higher average carbon concentration).

The general dependence of alloy 2 on the cooling rate was similar to that of alloy 1 although with its higher carbon concentration, most of the austenite decomposition occurred <320°C for $\dot{T} > 2$ K s^{-1} with fully martensitic microstructure, although a tiny amount of bainite could be seen at the decarburised surface. Fine bainite was observed for $\dot{T} < 2$ K s^{-1} (Fig. 6) but the microstructure also contained some martensite as inferred from the dilatometric curves, as shown in Fig. 3. Another difference with the lower carbon alloy was the degree of microstructural refinement: when comparing micrographs in Figs. 5 and 6, it is clear that finer bainite was obtained with the higher carbon content.

There is a refinement of microstructure in alloy 2, when compared with alloy 1, through the suppression of transformation to lower temperatures; this is evident by comparing the 50% reaction CCT curves for the two steels (Fig. 4). The difference is more obvious in the dilatometric plots in Fig. 7; the transformation begun at nearly the same temperature in both steels, but its development was suppressed in alloy 2 by ~50°C.

In summary, there is reasonable agreement between the calculated and measured CCT curves,

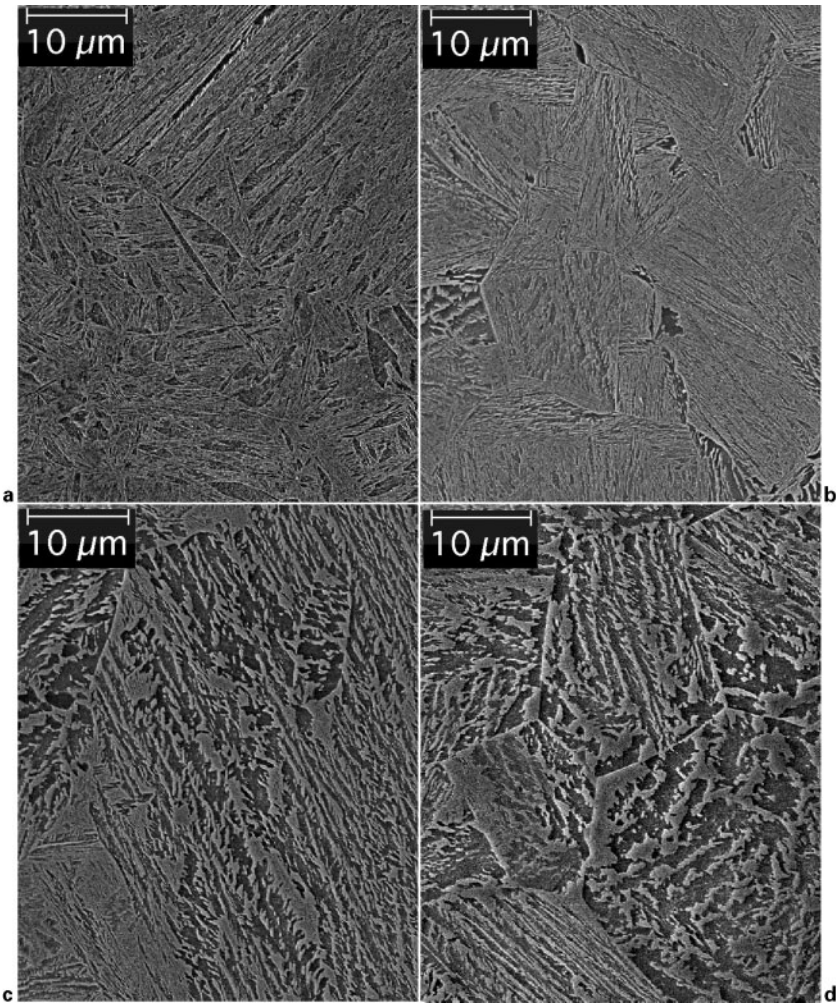

a 1 K s^{-1}; *b* 0·5 K s^{-1}; *c* 0·2 K s^{-1}; *d* 0·1 K s^{-1}

6 Alloy 2

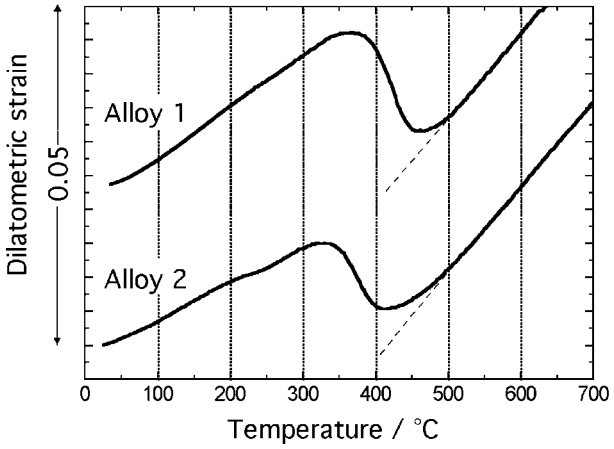

7 Dilatometric curves during cooling from 1000°C at 2 K s^{-1}

notwithstanding the small amount of transformation associated with the decarburised layers in the dilatometric samples. Table 2 contains a further comparison, where $\dot{T}_\alpha$ is the minimum cooling rate to avoid allotriomorphic ferrite, and $\dot{T}_{\alpha'}$ the minimum cooling rate needed to achieve a fully martensitic microstructure. It is particularly useful that the range of cooling rates in which bainite is the predominant transformation is correctly estimated.

Figure 8 shows the hardness data as a function of the alloy and cooling rate. The hardness expected from a fully martensitic microstructure is also plotted as a function of the cooling rate using an equation due to Maynier *et al.*[45] which accounts for the chemical composition of the steel and $\dot{T}$. The results confirm that the microstructure is essentially martensitic when $\dot{T} \geqslant 1$ K s^{-1}.

Table 2 Comparison of calculations (calc.) and measured (meas.) data from CCT diagrams.

	$\dot{T}_\alpha$, K s^{-1}		$\dot{T}_{\alpha'}$, K s^{-1}		M_S, °C		B_S, °C	
Steel	Calc.	Meas.	Calc.	Meas.	Calc.	Meas.	Calc.	Meas.
Alloy 1	0·25	0·2–0·5	8	>5	350–355	350	471	500
Alloy 2	0·22	0·2–0·5	6	2–5	330–340	320	446	500

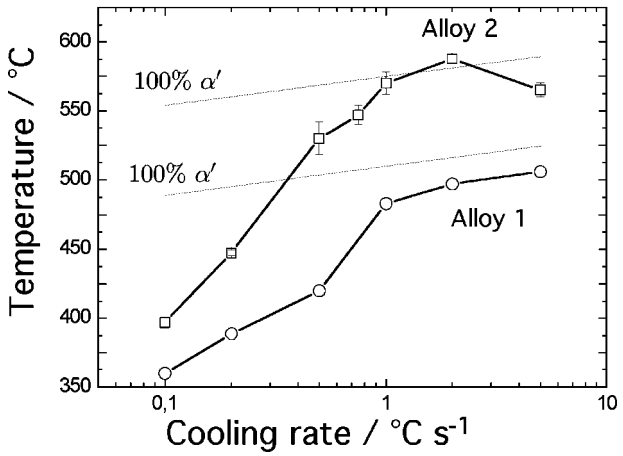

8 Hardness as function of cooling rate

Conclusions

It has been demonstrated that for a range of cooling rates appropriate in the manufacture of seamless pipes, a microstructure which consists mainly of bainite can be obtained in two alloys which differ only in the carbon concentration in the range 0·25–0·30 wt-%. The higher carbon concentration alloy is found to be more reliable in generating the required microstructure and has the additional advantage that the overall structure is finer.

As an additional outcome, the metallographic and kinetic measurements confirm the calculated continuous cooling transformation diagrams. The mechanical properties of the alloys are explored in Part 2 of the present paper.[36]

Acknowledgement

The authors are grateful to Tenaris Argentina (Research and Development) for funding this work.

References

1. A. A. Gorni and P. R. Mei: *J. Mater. Process. Technol.*, 2005, **162–163**, 298–303.
2. B. P. J. Sandvik and H. P. Nevalainen: *Met. Technol.*, 1981, **8**, 213–220.
3. H. K. D. H. Bhadeshia and D. V. Edmonds: *Met. Sci.*, 1983, **17**, 411–419.
4. H. K. D. H. Bhadeshia and D. V. Edmonds: *Met. Sci.*, 1983, **17**, 420–425.
5. V. T. T. Miihkinen and D. V. Edmonds: *Mater. Sci. Technol.*, 1983, **3**, 422–431.
6. V. T. T. Miihkinen and D. V. Edmonds: *Mater. Sci. Technol.*, 1987, **3**, 432–440.
7. V. T. T. Miihkinen and D. V. Edmonds: *Mater. Sci. Technol.*, 1983, **3**, 441–449.
8. L. Wenyan, Q. Jingxin and S. Hesheng: *J. Mater. Sci.*, 1997, **32**, 427–430.
9. A. Barbacki and E. Mikolajski: *J. Mater. Process. Technol.*, 1998, **78**, 18–23.
10. D. Y. Wei, J. L. Gu, H. S. Fang, B. Z. Bai and Z. G. Yang: *Int. J. Fatigue*, 2004, **26**, 437–442.
11. F. G. Caballero, M. J. Santofimia, C. Capdevila, C. Garcia-Mateo and C. G. de Andrés: *ISIJ Int.*, 2006, **46**, 1479–1488.
12. X. Fang, Z. Fan, B. Ralph, P. Evans and R. Underhill: *J. Mater. Sci.*, 2003, **38**, 3877–3882.
13. E. Dorazil, B. Barta, E. Munsterova, L. Stransky and A. Huvar: *AFS Int. Cast Met. J.*, 1982, **22**, 52–62.
14. D. J. Moore, T. N. Rouns and K. B. Rundman: *AFS Trans.*, 1985, **93**, 705–718.
15. V. Franetovic, A. Sachdev and E. F. Ryntz: *Metallography*, 1987, **20**, 15–36.
16. F. G. Caballero, H. K. D. H. Bhadeshia, K. J. A. Mawella, D. G. Jones and P. Brown: *Mater. Sci. Technol.*, 2001, **17**, 512–516.
17. F. G. Caballero, H. K. D. H. Bhadeshia, K. J. A. Mawella, D. G. Jones and P. Brown: *Mater. Sci. Technol.*, 2001, **17**, 517–522.
18. J. Deliry: *Mem. Sci. Rev. Metall.*, 1965, **62**, 527–550.
19. J. Pomey: *Mem. Sci. Rev. Metall.*, 1966, **63**, 507–532.
20. J. M. Schissler, J. Arnould and G. Metauer: *Mem. Sci. Rev. Metall.*, 1975, **72**, 779–793.
21. E. Kozeschnik and H. K. D. H. Bhadeshia: *Mater. Sci. Technol.*, 2008, **24**, 343–347.
22. S. B. Singh and H. K. D. H. Bhadeshia: *Mater. Sci. Eng. A*, 1998, **A245**, 72–79.
23. F. B. Pickering: Proc. 4th Int. Conf. on 'Electron microscopy', 626–637; 1958, Berlin, Springer Verlag.
24. F. B. Pickering: 'Physical metallurgy and the design of steels'; 1978, Essex, Applied Science Publishers.
25. S. Chatterjee and H. K. D. H. Bhadeshia: *Mater. Sci. Technol.*, 2006, **22**, 645–649.
26. F. G. Caballero and H. K. D. H. Bhadeshia: *Curr. Opin. Solid State Mater. Sci.*, 2005, **8**, 186–193.
27. H. K. D. H. Bhadeshia: *Met. Sci.*, 1982, **16**, 159–165.
28. H. K. D. H. Bhadeshia: *Met. Sci.*, 1981, **15**, 175–177.
29. H. K. D. H. Bhadeshia: *Met. Sci.*, 1981, **15**, 178–150.
30. J. W. Christian: 'Theory of transformations in metal and alloys, Part I', 3rd edn; 2003, Oxford, Pergamon Press.
31. S. A. Khan and H. K. D. H. Bhadeshia: *Metall. Trans. A*, 1990, **21A**, 859–875.
32. W. Jolley: *J. Iron Steel Inst.*, 1968, **206**, 170–172.
33. L. A. Norström and O. Vingsbo: *Met. Sci.*, 1979, **13**, 677–684.
34. C. L. Briant and S. K. Banerji: *Int. Met. Rev.*, 1978, **23**, (4), 164–199.
35. I. Olefjord: *Int. Met. Rev.*, 1989, **4**, 149–163.
36. G. Gomez, T. Pérez and H. K. D. H. Bhadeshia: *Mater. Sci. Technol.*, DOI: 10.1179/174328408X388149.
37. 'Standard test methods for notched bar impact testing of metallic materials', E23 07a, ASTM, Pennsylvania, PA, USA, 2007.
38. H. K. D. H. Bhadeshia and D. V. Edmonds: *Met. Sci.*, 1979, **13**, 325–334.
39. F. G. Wilson and T. Gladman: *Int. Mater. Rev.*, 1988, **33**, 221–286.
40. K. D. Walker and R. I. Marshall: *Mater. Sci. Technol.*, 1990, **6**, 867–871.
41. T. Gladman: *Heat Treat. Met.*, 1994, **21**, 11–14.
42. M. F. Eldridge and R. C. Cochrane: *Mater. Sci. Forum*, 1998, **284–286**, 217–224.
43. K. W. Andrews: *J. Iron Steel Inst.*, 1965, **203**, 721–727.
44. R. T. DeHoff and F. N. Rhines: 'Quantitative microscopy'; 1968, New York, McGraw Hill.
45. P. Maynier, B. Jungmann and J. Dollet: in 'Hardenability concepts with applications to steels', (ed. D. V. Doane and J. S. Kirkaldy), 518–545; 1978, Materials Park, OH, TMS–AIME.